◆ Human Brain Mapping 37:3003–3016 (2016) ◆

# Functional Organization of the Fusiform Gyrus Revealed with Connectivity Profiles

**Wen Zhang,[1,2] Jiaojian Wang,[1] Lingzhong Fan,[3] Yuanchao Zhang,[1] Peter T. Fox,[4] Simon B. Eickhoff,[5,6] Chunshui Yu,[7] and Tianzi Jiang[1,3,8,9,10]***

[1]*Key Laboratory for NeuroInformation of the Ministry of Education, School of Life Science and Technology, University of Electronic Science and Technology of China, Chengdu, China*
[2]*School of Computing, Informatics, and Decision Systems Engineering, Arizona State University, Tempe, AZ, USA*
[3]*Brainnetome Center, Institute of Automation, Chinese Academy of Sciences, Beijing, China*
[4]*Research Imaging Institute, University of Texas Health Science Center at San Antonio, Texas*
[5]*Institute of Neuroscience and Medicine (INM-1), Research Centre Jülich, Germany*
[6]*Institute of Clinical Neuroscience and Medical Psychology, Heinrich Heine University, Dusseldorf, Germany*
[7]*Department of Radiology, Tianjin Medical University General Hospital, Tianjin, China*
[8]*National Laboratory of Pattern Recognition, Institute of Automation, Chinese Academy of Sciences, Beijing, China*
[9]*The Queensland Brain Institute, University of Queensland, Brisbane, QLD, Australia*
[10]*CAS Center for Excellence in Brain Science and Intelligence Technology, Institute of Automation, Chinese Academy of Sciences, Beijing, China*

**Abstract:** Within the object recognition-related ventral visual stream, the human fusiform gyrus (FG), which topographically connects the striate cortex to the inferior temporal lobe, plays a pivotal role in high-level visual/cognitive functions. However, though there are many previous investigations of distinct functional modules within the FG, the functional organization of the whole FG in its full functional heterogeneity has not yet been established. In the current study, a replicable functional organization of the FG based on distinct anatomical connectivity patterns was identified. The FG was parcellated into medial (FGm), lateral (FGl), and anterior (FGa) regions using diffusion tensor imaging. We validated the reasonability of such an organizational scheme from the perspective of resting-state whole brain functional connectivity patterns and the involvement of functional subnetworks. We found corroborating support for these three distinct modules, and suggest that the FGm serves as a transition region that combines multiple stimuli, the FGl is responsible for categorical recognition, and the FGa is involved in semantic understanding. These findings support two organizational functional transitions of the ventral temporal gyrus, a posterior/anterior direction of visual/semantic processing, and a

Contract grant sponsor: National Basic Research Program of China (973 program); Contract grant number(s): 2012CB720702, 2011CB707801; Contract grant sponsor: Strategic Priority Research Program of the Chinese Academy of Sciences; Contract grant number: XDB02030300; Contract grant sponsor: Natural Science Foundation of China; Contract grant number(s): 91432302, 91132301

*Correspondence to: Tianzi Jiang, Brainnetome Center, Institute of Automation, Chinese Academy of Sciences, Beijing, China.
E-mail: jiangtz@nlpr.ia.ac.cn

Received for publication 13 October 2015; Revised 6 April 2016; Accepted 10 April 2016.

DOI: 10.1002/hbm.23222

Published online 2 May 2016 in Wiley Online Library (wileyonlinelibrary.com).

media/lateral direction of high-level visual processing. Our results may facilitate a more detailed study of the human FG in the future. *Hum Brain Mapp 37:3003–3016, 2016.* 

**Key words:** parcellation; fusiform gyrus; functional characterization; resting-state; tractography

## INTRODUCTION

The fusiform gyrus (FG), located in the middle of the ventral temporal lobe (VTL), is one of the most important brain areas in the visual ventral stream. It has been well established that the FG participates in a range of visual cognitive functions, such as facial recognition [Kanwisher et al., 1997; Sergent et al., 1992], body parts discrimination [Peelen and Downing, 2005; Taylor et al., 2007], and recognition of various object features [Schwarzlose et al., 2008; Wang et al., 2013]. Several studies have indicated that the functional activity of the FG is highly associated with language processing [Cohen et al., 2000; Dehaene et al., 2001; Mion et al., 2010], which, when considered with the fact that visual information decoding occurs along the posterior–anterior axis of the VTL, suggests that complex semantic knowledge processing occurs in this area. In addition to these important functional characteristics of the FG, an asymmetrical functional profile has been identified in the bilateral posterior FG [Balsamo et al., 2006; Caspers et al., 2013a]. Its complex and diverse functions suggest the possibility of a more fine-grained functional organization scheme in the FG.

It is worth noting that the strong category-selective neural representations of the face and body and the perception of objects reported by many functional MRI (fMRI) studies of the human FG were limited to the posterior-lateral FG [Kanwisher and Yovel, 2006, Price and Devlin, 2003, Taylor et al., 2007]. However, the specific functional role of other parts of the FG in the ventral visual stream remains unclear. Earlier cytoarchitectonic and myleoarchitectonic atlases described the FG as a uniform area. Recent studies subdivided the posterior part of the FG into the medial FGm and the lateral FGl based on different cytoarchitectonic properties and different distribution patterns of receptors [Caspers et al., 2013a,b] and they further divided the mid-fusiform gyrus into two cytoarchitectonic subregions [Lorenz et al., 2015]. Although cytoarchitectural or myleoarchitectural approaches can characterize detailed local properties of cortical areas, their connectivity information, especially their long-range connectivity, which is what actually determines the functions with which an area is involved [Eickhoff et al., 2010; Passingham et al., 2002] remains unclear. However, diffusion tensor imaging (DTI) combined with fMRI techniques is able to document the fiber connection patterns of the FG and to further estimate its functional organization. In fact, researchers in this area have successfully utilized DTI with fMRI to explore the subdivisions of many brain regions and have showed that they are highly consistent with traditional cytoarchitectonic findings [Beckmann et al., 2009; Fan et al., 2013; Mars et al., 2012; Wang et al., 2012; Zhang et al., 2014].

In this research, we first used DTI data to parcellate the FG for the purpose of identifying distinct anatomical connectivity patterns. Then, we explored the functional role of each FG subregion by identifying their (1) whole brain resting-state functional connectivity patterns, (2) network-based connectivity properties. Eventually, we uncovered the details of the functional organization of the FG that could properly describe both its anatomical and its functional heterogeneity.

## MATERIAL AND METHODS

### Subjects

#### *Dataset 1*

Twenty healthy, right-handed subjects were recruited for anatomical connectivity-based parcellation (10 males and 10 females; age [mean ± standard deviation], 23.0 ± 1.8; range 19–25 years). The same data from these subjects were used in a previous study [Zhang et al., 2014]. Subjects with a history of brain injury, potential mental disorders, or conditions incompatible with an MRI scan were excluded. All subjects in this study signed a written, informed consent form that had been approved by the medical research ethics committee of Tianjin Medical University.

#### *Dataset 2*

To provide a replication dataset, a completely independent group of 20 healthy, right-handed subjects were recruited from the University of Electronic Science and Technology of China (UESTC; 10 males and 10 females; age (18.6 ± 0.7; range 18–20 years). In keeping with Dataset 1, subjects with a history of brain injury, potential mental disorder, or conditions incompatible with an MRI scan were excluded. Before scanning, all subjects signed a written informed consent form that was approved by the local ethics committee of UESTC.

### Data Acquisitions

All the subjects from Dataset 1 were scanned using a SignaHDx 3.0 Tesla MR scanner (General Electric, Milwaukee, WI). The DTI contained 55 images with noncollinear diffusion gradients ($b = 1{,}000$ s/mm$^2$) and three nondiffusion-weighted

**TABLE I. Scanning parameters for the two datasets**

| Dataset | Scan | TR (ms) | TE (ms) | FOV (mm) | Matrix | Number of slices | Slice thickness (mm) |
|---|---|---|---|---|---|---|---|
| Dataset 1 | T1 | 8.1 | 3.1 | 256 | 256*256 | 176 | 1 |
| | DTI | 10,000 | 64.2 | 256 | 128*128 | 45 | 3 |
| | FMRI | 2,000 | 30 | 240 | 64*64 | 40 | 4 |
| Dataset 2 | T1 | 8.1 | 3.1 | 256 | 256*256 | 188 | 1 |
| | DTI | 8,500 | 67.6 | 256 | 128*128 | 75 | 2 |

images ($b = 0$ s/mm$^2$) using a single-shot echo planar imaging sequence. Echo-planar imaging blood oxygen level-dependent images of the whole brain were acquired in 40 axial slices and each functional run lasted 6 min (180 volumes); sagittal 3D T1-weighted images were acquired with a brain volume (BRAVO) sequence. Dataset 2 was scanned using a 3.0 Tesla GE MR Scanner. The DTI data included 64 images with non-collinear diffusion gradients and three nondiffusion-weighted images. Sagittal 3D T1-weighted images were also acquired in Dataset 2. Table I shows the details of scanning parameters for the two Datasets.

## Data Analysis

The diffusion and structural images were processed using the FMRIB's Diffusion Toolbox 4.0 (FSL, http://fsl.fmrib.ox.ac.uk/fsl) and the MINC toolbox (http://www.bic.mni.mcgill.ca/ServicesSoftware/MINC). Briefly, the structural MR images were corrected for nonuniformity artifacts using the nonparametric nonuniform intensity normalization (N3) algorithm. Following skull-stripping (brain extraction) for all images, the T1-weighted scans were linearly coregistered onto the nondiffusion b0 images. The anatomical scans (coregistered into native diffusion space) were then spatially normalized to Montreal Neurological Institute (MNI) template space using a linear and nonlinear transformation, as provided by the MINC toolbox. The ensuing deformation parameters were subsequently used to transfer the FG mask from the template space to the individual diffusion space.

The preprocessing of the resting state fMRI data was performed using the scripts provided by the 1,000 Functional Connectomes Project (http://www.nitrc.org/projects/fcon_1000) [Biswal et al., 2010] using both the FSL and AFNI (Automated Functional Neuroimaging; http://afni.nimh.nih.gov/afni) software. In brief, the preprocessing steps were as follows: (1) discarding the first 10 volumes in each scan series to allow for signal equilibration, (2) slice-timing correction for the remaining images, (3) performing motion correction, (4) time series despiking, (5) spatial smoothing with a Gaussian kernel of 6 mm full-width at half maximum (FWHM), (6) normalizing the mean-based intensity, (7) temporal band-pass filtering (0.01–0.08 Hz), (8) removing linear and quadratic trends, (9) structural MR image processing including brain masking, tissue classification, linear and nonlinear spatial normalization to the MNI152 brain template and other anatomical data processing steps, (10) coregistering the anatomical volume with the mean functional volume, (11) performing nuisance signal regression (nuisance signals from white matter, cerebrospinal fluid, the global signal, and six motion parameters), and, finally, (12) resampling of the functional data into MNI space with the concatenated transformations. In the end, a 4-dimensional (4D) residual time series dataset was built for each participant in standard MNI space. Moreover we examined the signal-to-fluctuation-noise-ratio (SFNR) to validate the signal quality of the fMRI data (Fig. 1).

## Definition of the FG Boundary

The boundary of the FG was defined according to the Destrieux Atlas [Destrieux et al., 2010], which is a standard anatomical template that reflects sulco-gyral structures (Fig. 2). The Destrieux Atlas based on the surface-based coordinate systems, which is suggested to be more appropriate for the anatomy of the brain than classical volume-based coordinate systems [Destrieux et al., 2010]. This atlas was acquired using a computer-assisted automated method which was showed to be both anatomically valid and reliable [Destrieux et al., 2010]. It captures the core topological properties of the cortical folding while neglects variations of the complex sulco-gyral organization across individuals thus allows the highly accurate intersubject comparison [Destrieux et al., 2010]. Moreover it contains more topological information and provides a more precise description of the cortical surface than the gyral-based atlas, such as "Desikan-Killiany" cortical atlas [Desikan et al., 2006] in FreeSurfer. The FG, also named the lateral occipito-temporal gyrus, is grossly quadrangular. It is anterior-laterally bordered by the anterior transverse collateral sulcus and posterior-laterally bordered by the posterior transverse collateral sulcus. The medial and lateral walls are, respectively, defined by the medial occipito-temporal sulcus and the lateral occipito-temporal sulcus [Destrieux et al., 2010]. It is worth noting that this atlas avoids including the anterior transverse collateral sulcus, which connects to the temporal pole as part of the anterior FG. Previous research studies using DTI-based fiber tracking and resting state fMRI analysis, respectively, demonstrated clear differences in the structural and functional

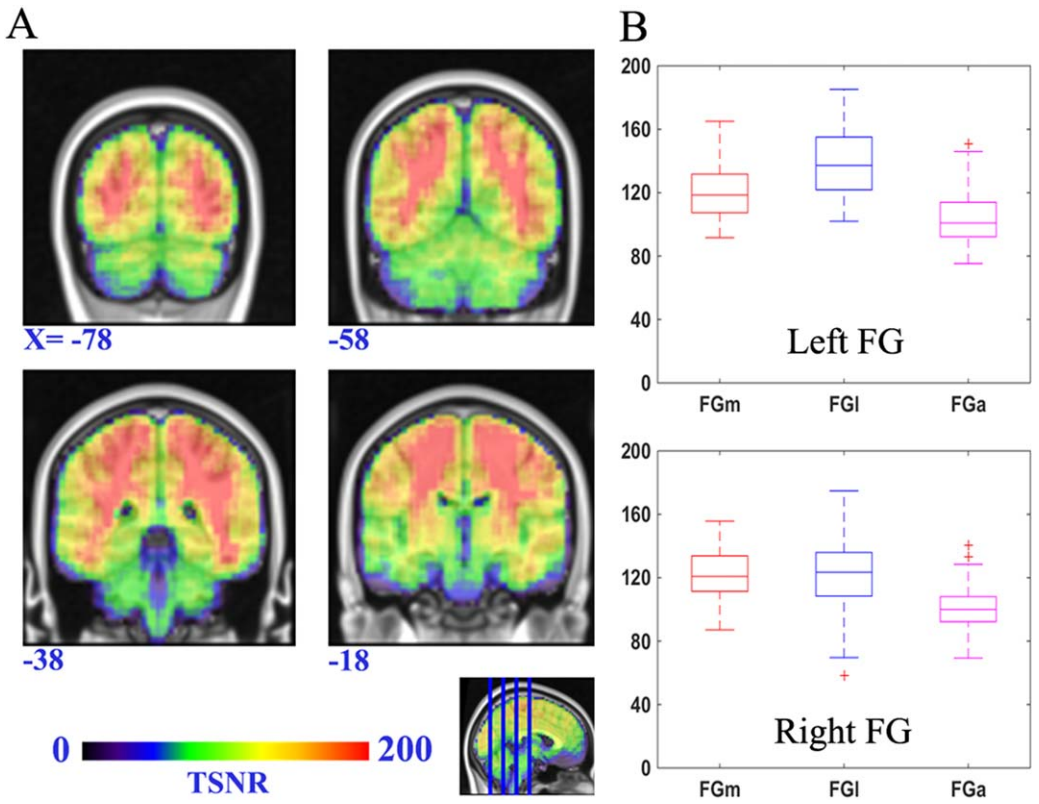


**Figure 1.**
The SFNR map across the FG. The left subfigure (**A**) is a map of the SFNR value onto the standard brain template (MNI space) such that warmer colors indicate a higher SFNR value. The right subfigure (**B**) shows the distribution of the SFNR value for voxels in each FG subregion.

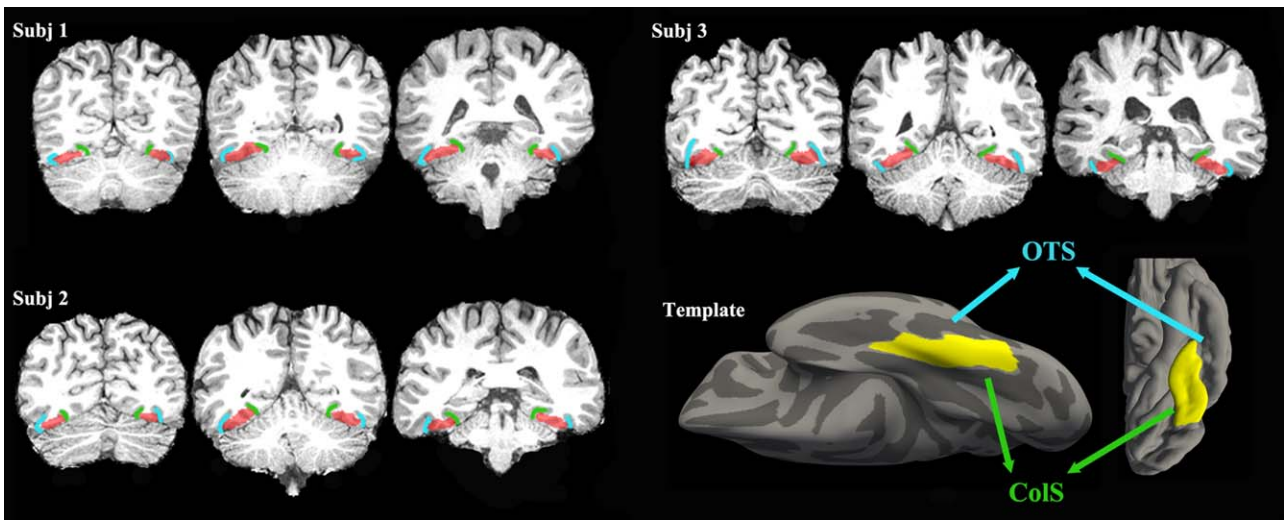


**Figure 2.**
Three examples of the FG mask in individual space. The right corner shows a surface view of the defined FG template. The blue line indicates the occipito-temporal sulcus, and the green line indicates the collateral sulcus.

connection patterns between the gyri and sulci [Deng et al., 2014; Nie et al., 2012].

We constructed the FG seed mask using a method that formed group probability maps. Basically, for each subject, we extracted the individual FG mask on the gray/white matter boundary based on the Destrieux Atlas using FreeSurfer software (http://surfer.nmr.mgh.harvard.edu/). Next the vertexes on the binary mask were inflated both inwardly (2 mm) and outwardly (1 mm) along the gray/white matter boundary to form a voxel mask (3 mm ribbon) in native space. Each inflated mask was visually inspected and manually corrected to ensure the accuracy of the mask boundary. Then, each individual binary FG mask was mapped to standard space. To combine the individual masks (20 people) into one, we extracted and chose all the voxels that were identified in more than 10 people (50% probability) to form the group mask of the FG. Finally, we applied the transformation matrix from the T1 images transformation to the group mask in standard space and re-obtained new individual FG masks in native DTI space for probabilistic fiber tracking. Figure 2 shows several examples of the individual FG masks. The way we did the group-based FG mask before tractography was advantageous in that it was able to evaluate the distribution of all the voxels in the FG in advance and was able to exclude subjects who had a relatively large anatomical variation in the FG. Additionally, we kept the voxels that occurred in most of the individual masks. Thus, it was able to primarily focus on those voxels rather than on the rest of the voxels which were only identified in a few masks. Moreover, it was more convenient to draw a probability-based conclusion in the end.

## Connectivity-Based Parcellation

The probabilistic fiber tracking was performed in native diffusion space to estimate the voxelwise probability distribution, which was calculated using a multiple fiber extension [Behrens et al., 2007] obtained from a previously published diffusion modeling approach [Behrens et al., 2003]. Probability tractography was carried out by sampling 5,000 streamline fibers per voxel without a distance correction. The connectivity probability maps between a specific voxel (voxel $i$) in the seed region (left and right FG separately) and every voxel in the target region (the whole brain mask) were defined by the number of traces arriving at the target site from that voxel (voxel $i$) in the seed region. We then thresholded the connectivity probability maps by removing those voxels that had fewer than 10 out of 5,000 traces and further down-sampled each map to a lower resolution with a voxel size of $5 \times 5 \times 5$ mm. Moreover, based on connectivity profiles, we calculated the cross-correlation between every pair of seed voxels and obtained a symmetric matrix revealing any similar patterns in structural connectivity for each subject.

In this study, we used a spectral clustering algorithm with edge-weighted centroidal voronoi tessellations segmentation to group the voxels of the FG that had similar connectivity patterns. This modified spectral clustering algorithm maintained the integrity of the clusters primarily by removing the small discrete voxels [Wang et al., 2012]. Based on the spatial constraint, the clustered voxels were reassigned iteratively to their nearest clusters by considering both the Euclidean distance between the voxels and each cluster's center and the clustering information of their neighboring voxels. This process was continued until the location of each cluster's center remained unchanged. After obtaining the clustering results for each subject in individual space, we transformed them into MNI standard space and created a maximum probability map (MPM) to visualize the group FG parcellation scheme.

To identify the optimal clustering numbers, we evaluated them using both within-group and between-group analyses to avoid an arbitrary conclusion. First, cross-validations were applied to determine the similarity of the parcellation results within Dataset 1 for all clusters. The tested cluster number ranged from 2 to 7. We evaluated the similarity using Cramer's V (CV) over the interval 0-1, in which a higher value indicated greater consistency. Second, after deciding the clustering number based on the highest CV value, we repeated this process on Dataset 2 using the identical method to explore the reproducibility between the different datasets. If the clustering results from the two datasets were consistent, we could conclude that the choice of the clustering number was reasonable and accept it.

## Mapping Whole Brain Anatomical Connectivity Patterns

To obtain the whole brain anatomical connectivity patterns, we extracted each subregion that had a minimum probability of 50% from the probability maps of the FG as the seed areas for probabilistic tractography. This map of the connectivity patterns was designed to present the fiber connections that drove the parcellation scheme. To reduce the number of false probability connections, two threshold levels were used. At the individual level, a conservative threshold value of $P > 0.0004$ was used to remove voxels that had a very low connectivity probability. Next, at the group level, only the fiber tracks that were consistently identified in standard space in more than 50% of the subjects were maintained to form the population maps.

## Functional Connectivity Analysis of the FG Subregions

The seed definition for the FG subregions was the same as the one used in processing the anatomical connectivity maps (thresholded using 50% probability). Then, each subregion seed was multiplied by the gray matter mask to

ensure that all the voxels in each seed were within the gray matter. To obtain valid functional activity patterns for each FG subregion, we followed two different procedures to perform a functional connectivity analysis.

In the first procedure, we mapped the whole brain functional connectivity pattern for each FG subregion. First, we resampled the seed subregion masks to obtain a 3 mm resolution and averaged the time series of all the voxels within each seed area. Then, the Pearson correlations were calculated between the averaged time series of each seed and that of voxels in the whole brain mask. Next, the correlation coefficients for each pair of seed-to-target connections were converted to *z*-scores using Fisher's *Z*-transform to improve normality. Finally, a one-sample *t*-test and a paired *t*-test were performed to determine the functional connectivity patterns for each subregion and to show any differences in the functional connectivity strengths between the different seed areas. For the above voxel-wise comparisons, the false discovery rate (FDR) method was applied for a multiple comparison correction ($P < 0.05$), and only clusters containing a minimum of 50 voxels were retained for consideration.

In the second procedure, we established the functional connectivity fingerprints between the FG subregions and ten functional subnetworks. The 10 networks were those which revealed functional correspondence between the rest- and task-states [Smith et al., 2009] and can be used more specifically and straightforwardly than whole brain functional connectivity to describe the distinct functional participation of each FG subregion in the resting state. They are the: (1) medial visual areas network (MVAN), (2) occipital pole visual areas network (OPVAN), (3) lateral visual areas network (LVAN), (4) default mode network (DMN), (5) cerebellum (CN), (6) sensorimotor network (SN), (7) auditory network (AN), (8) executive control network (ECN), (9) perception network (PN), and (10) language cognition network (LCN). Here, we also calculated the average time series for each seed area and for each subnetwork. For each seed-to-network pair, the functional connectivity was computed using a Pearson correlation and was then averaged across all the subjects. The results were used to generate functional connectivity fingerprints.

## RESULTS

### Connectivity-Based Parcellation Scheme

Based on the different connectivity patterns derived from probabilistic tractography using in vivo DTI data, we subdivided the FG into three subregions in each subject's individual space. The consistent coefficients in Figure 3 show that the three subregions scheme remained the most stable (highest value) in Dataset 1 when $k$ ranged from 2 to 7. A maximum probability map for each of these 3 FG subregions was created in standard MNI space (Fig. 4A). The regions included the medial part of the FG (FGm, green), the lateral part of the FG (FGl, blue), and the anterior FG (FGa, red). The FGm and FGl were divided by the mid-fusiform sulcus from its posterior to anterior tip and were similar to but larger than the FG1 area and the FG2 area defined by Caspers et al. [2013b] using cytoarchitecture. The FGa was located anterior to the FGm and FGl and lateral to the parahippocampus. Applying the identical parcellation method, Dataset 2 showed a similar organizational scheme when $k = 3$ (see Fig. 4B). In addition, the probability distribution for each subregion was calculated to characterize the individual variability (Fig. 4C,D).


**Figure 3.**
Using Cramer's V as an indication of the clustering consistency (interval 0-1), where larger values indicate high consistency and "1" stands for the perfect match, we found that the three cluster solution showed a significantly higher value than other solutions. [Color figure can be viewed in the online issue, which is available at wileyonlinelibrary.com.]

### Whole Brain Anatomical Connectivity Patterns

Two major fiber bundles were distinguished using the whole brain probabilistic fiber tractography of the FG (Fig. 5). These were the inferior longitudinal fasciculus (ILF) and inferior fronto-occipital fasciculus (IFOF), both of which traveled longitudinally along the posterior–anterior axis. The FGm primarily connected with the striate and extrastriate cortex and the FGl predominantly connected with the lateral temporal and occipital regions by means of these two large fiber bundles. The FGa showed strong connections with the hippocampus and inferior temporal gyrus. More specifically, we found out that the medial/lateral split was primarily driven by the vicinity of the two large fiber bundles (IFOF and ILF), the anterior/posterior split was primarily decided by its direct connection to the IFOF and ILF, and the anterior part had more connections to the IFOF but less to the ILF compared with the posterior part. Moreover, we performed an ROI-to-FG subregion connectivity analysis (the ROI regions were those defined using the AAL template) but did not find a significant difference between the anatomical connectivity patterns of the FG regions to the ROIs (especially in the

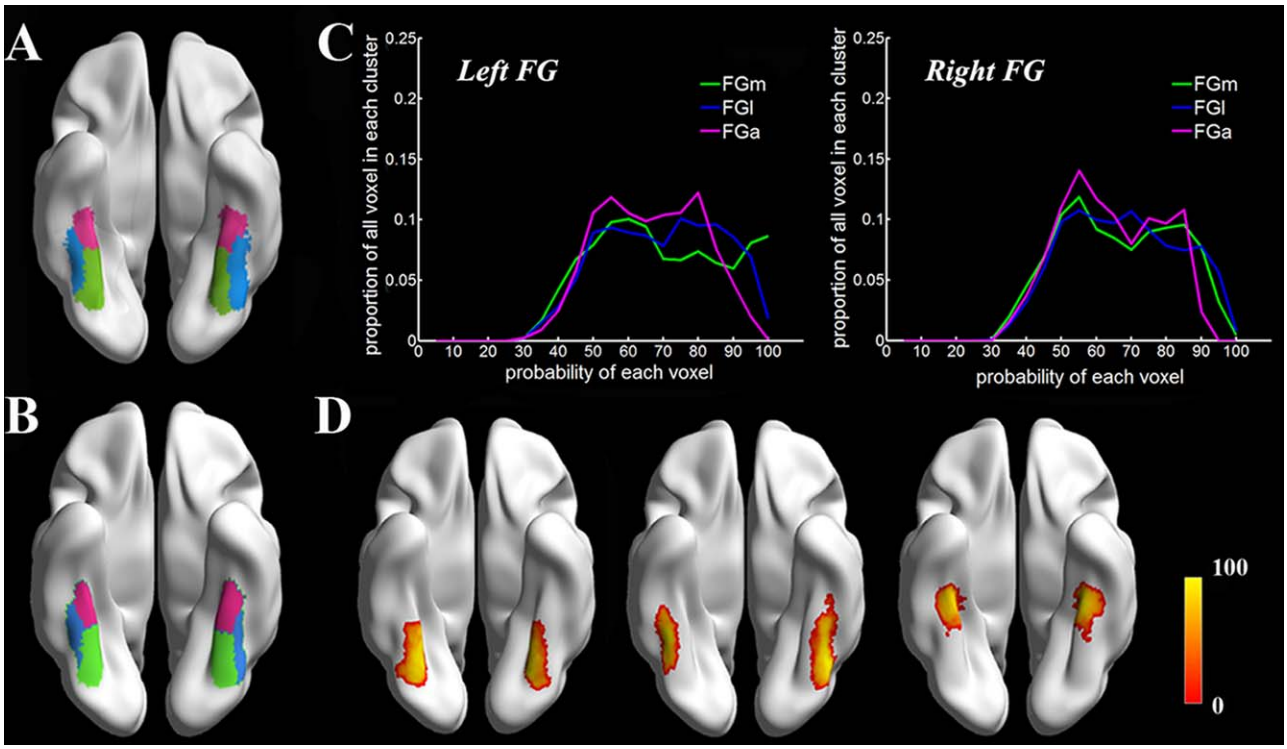


**Figure 4.**

Our connectivity-based parcellation scheme of the FG. The results from Dataset 1 and Dataset 2 are presented in Figures 4A,B, respectively. The FGm refers to the medial portion of the FG (green. MNI space, −29,-57,-14 for left; 31,-57,-15 for right); the FGl refers to the lateral portion of the FG (blue. MNI space, −42,-52,-20 for left; 42,-51,-21 for right), and the FGa refers to the anterior FG (red. MNI space, - 36,-32,-23for left; 35,-33,-23 for right). Figure 4C indicates the proportion of voxels in the cluster at a certain probability value, and Figure 4D shows the mapping result of the probability distribution for the three subregions with color map-encoded probability values.

frontal or parietal cortex) except for the connections that were to ROIs in the vicinity of the FG (e.g., the parahippocampal gyrus and inferior temporal gyrus).

### Whole Brain Functional Connectivity Patterns

We tested the fMRI signal quality before doing the whole brain functional connectivity analysis. **Figure** 1 shows that the major voxels in the FG had large SFNR values (much greater than 0) and that the mean SFNR value of each FG subregion was more than 100. This indicates that the FMRI signal in the FG seed area was not affected by artifacts; thus, the functional connectivity pattern drawn from this dataset seems to be a reliable way to explore the implicit functional roles of clusters. In the current study, we mapped the whole brain resting-state functional connectivity (rsFC) patterns of each subregion to identify the functional networks with which each was possibly involved (Fig. 6). In Figure 6, we showed such functional patterns for left (A) and right (B) FG subregions, respectively (FGm, FGl, and FGa) after correcting the multiple comparison with FDR ($P < 0.05$) and a cluster extent threshold (cluster size greater than 50 vexels), where in the figure, the red/yellow color indicates the positive correlations and blue color indicates the negative correlations. Different functional connectivity patterns were found for each subregion. The medial subregion, the FGm, was positively correlated with the postcentral gyrus, superior temporal gyrus, occipital pole, and posterior insula and negatively correlated with the supramarginal gyrus and the middle frontal gyrus as well as with the medial superior frontal gyrus. The lateral subregion, the FGl, was primarily positively correlated with the superior parietal gyrus, middle frontal gyrus, posterior part of the lateral superior frontal gyrus, supramarginal gyrus, lateral occipital gyrus, and middle insula. In addition, negative functional connectivity with the lateral and medial superior frontal gyrus, inferior parietal gyrus, middle temporal gyrus, and posterior cingulate cortex was found. The anterior FGa showed a positive rsFC with the precuneus, middle temporal gyrus, middle occipital area, and lateral superior frontal gyrus as well as negative rsFC with the

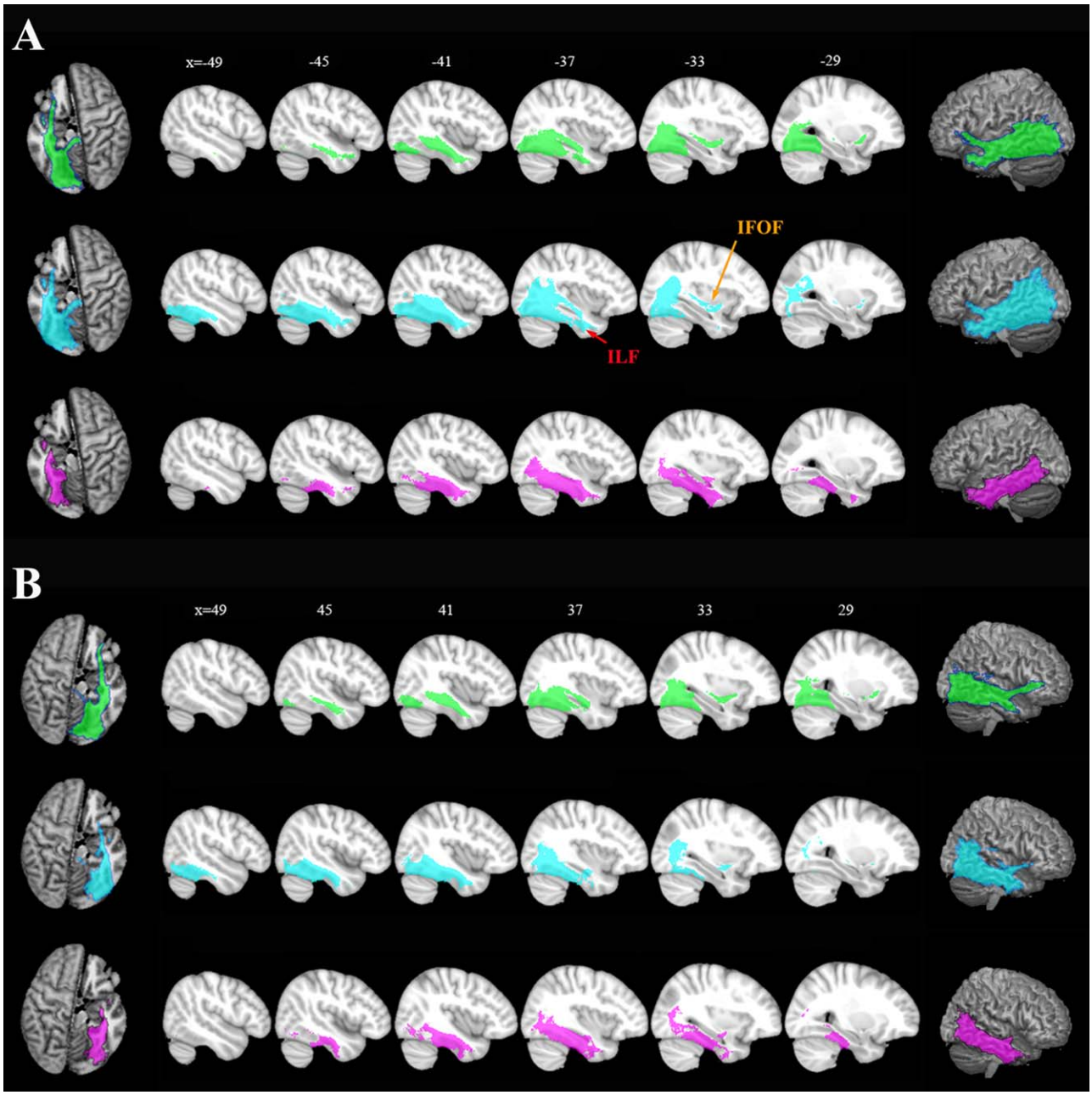


**Figure 5.**

Population maps of the whole brain anatomical connectivity patterns from the left (A) and right (B) hemispheres. FGm (green), FGl (blue), and FGa (red). The probability fiber tracks were projected back to the anatomical MNI space and averaged for the same cluster. Two major fiber bundles, IFOF and ILF, were identified and marked. The results are displayed using MRIcron. [Color figure can be viewed in the online issue, which is available at wileyonlinelibrary.com.]

anterior insula, medial superior frontal gyrus, occipital pole, and precentral gyrus. The bilateral FG subregions, except for the FGl, showed similar positive and negative rsFC patterns. The left FGl had a positive connection with the bilateral middle frontal gyrus that was not found for the right FGl.

## Resting-State Functional Connectivity Fingerprints

In this study, we also evaluated the rsFC of each FG subregion using ten predefined functional subnetworks (Fig. 7) to see if we could further support the whole brain

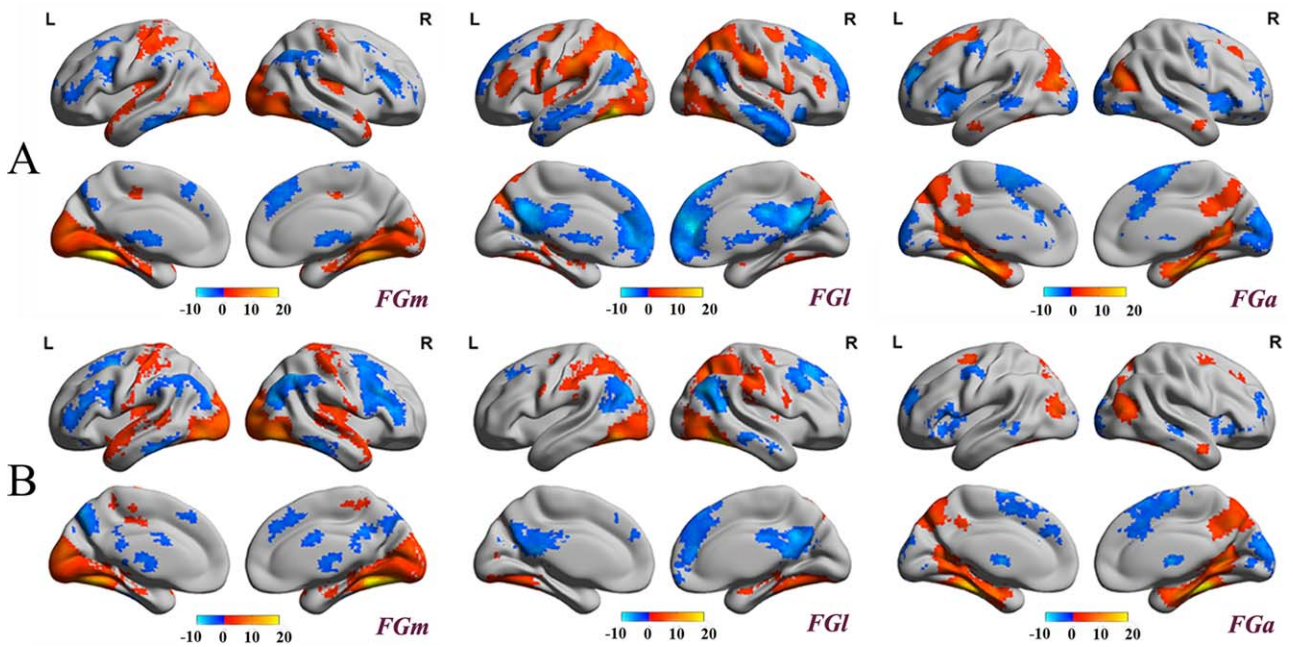


**Figure 6.**

Spatial distribution of the whole brain rsFC patterns for the left (A) and right (B) FG subregions. Statistical parametric maps are displayed using a voxel-level statistical threshold of $P < 0.05$ (FDR correction) with a cluster extent threshold of 50 voxels. The blue color indicates negative correlations and the red/yellow color represents positive correlations. The result shows the distinct functional connectivity patterns of 3 FG subregions in both hemispheres.

rsFC pattern maps and could better characterize the functional connectivity properties. The network connectivity fingerprints showed different connectivity properties for each subregion, a finding which further validated our parcellation results. The bilateral FGm showed a high correlation with subnetworks related to visual (Left FGm: MVAN, positive correlation value $R = 0.38$; OPVAN, $R = 0.44$; LVAN, $R = 0.35$. Right FGm: MVAN, $R = 0.44$; OPVAN, $R = 0.51$; LVAN, $R = 0.42$) and auditory (Left FGm: AN, $R = 0.26$. Right FGm: AN, $R = 0.32$) signal processing. The FGl showed a lateralized tendency, in that the left FGl was positively correlated to the functional subnetworks responsible for visual-language (OPVAN, $R = 0.45$; LVAN, $R = 0.37$; LCN, $R = 0.36$) and perception paradigms (PN, $R = 0.26$), whereas the right FGl showed a much weaker positive correlation with the language and perception networks (LCN, $R = 0.14$) but a strongly positive correlation with the visual networks (OPVAN, $R = 0.44$; LVAN, $R = 0.35$). In addition, the FGa had a notable positive connection with the DMN (Left FGa: DMN, $R = 0.29$. Right FGa: DMN, $R = 0.26$). Those results showed the low-level visual processing of FGm because of the relation to 3 visual networks, MVAN, OPVAN, LVAN, while the higher level visual processing, that is, language cognition or semantic understanding, was mainly processed by FGl and FGa due to the high correlation with LCN or DMN.

## DISCUSSION

In the present study, a reliable functional organization of the human FG was deduced using a DTI-based parcellation method based on probabilistic fiber tractography on two independent datasets. Three distinct subregions, consisting of the medial (FGm), lateral (FGl), and anterior (FGa), and their characteristic structural and functional connections were identified. By utilizing whole brain connectivity maps for the FG subregions and database driven functional characterization, we were able to assess their potential roles in processing and interpreting visual information.

The parcellation topography of the FG derived from DTI in this study was consistent with the previous cytoarchitectonic map obtained from ten postmortem human brains by Caspers and his colleagues [Caspers et al., 2013b]. They reported a medial-lateral scheme in the posterior FG that contained two distinct cytoarchitectonic areas (FG1 and FG2). These two subregions were anterior to the hOC4v (V4) in the ventral visual area and located within the FGl and FGm in our results. The FG1 composed the posterior part of FGm in our scheme which is located lateral to the retinotopically defined areas VO-1 and VO-2 [Arcaro et al., 2009; Brewer et al., 2005]. The posterior part of FGl corresponding to the FG2 is located posterior and dorsal to

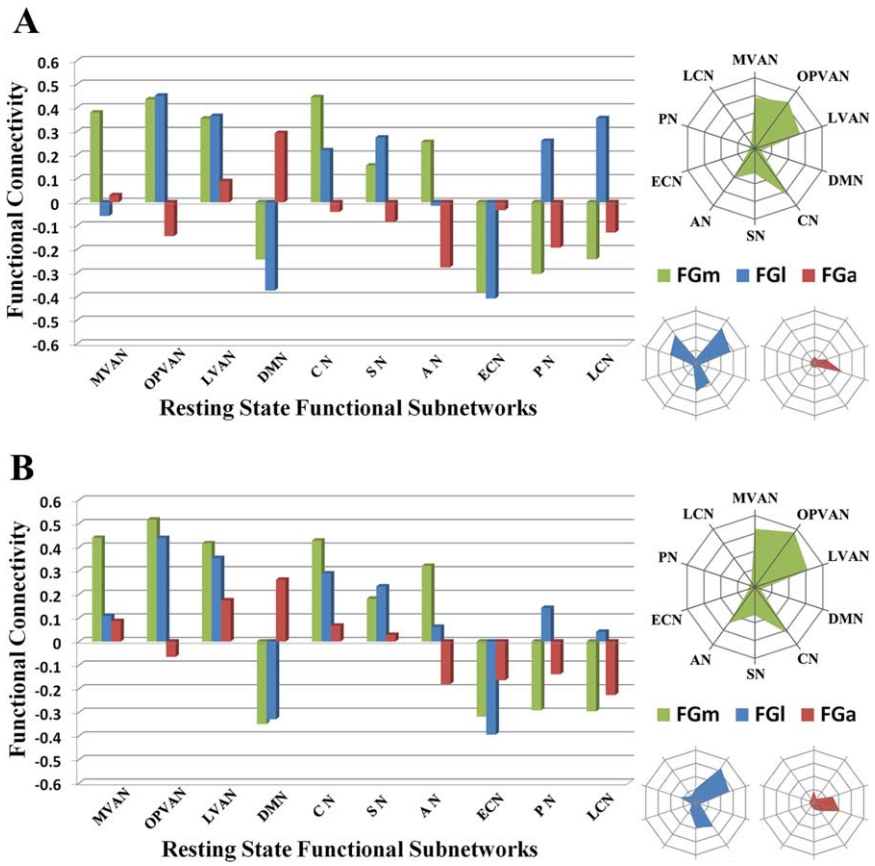


**Figure 7.**

The rsFC fingerprints associated with 10 functional subnetworks for the left (**A**) and right (**B**) FG subregions. The ten functional subnetworks are the: (1) medial visual areas network (MVAN), (2) occipital pole visual areas network (OPVAN), (3) lateral visual areas network (LVAN), (4) default mode network (DMN), (5) cerebellum (CN), (6) sensorimotor network (SN), (7) auditory network (AN), (8) executive control network (ECN), (9) perception network (PN), and (10) language cognition network (LCN). The quantitative reFC results for the different FG subregions with each target subnetwork are shown on the bar graphs and the tendencies of the positive connections are expressed via radar graphs for the left FGm (green), FGl (blue), and FGa (red). [Color figure can be viewed in the online issue, which is available at wileyonlinelibrary.com.]

another retinotopic region phPIT [Kolster et al., 2010] on the inferior temporal gyrus. Recently, the extended study of the cytoarchitectonic segregation in the mid-fusiform gyrus (mFG) identified two new areas, FG3 and FG4, which were rostral to FG1 and FG2, respectively [Lorenz et al., 2015]. Compared to our study, the FG1 and FG3 constitute the area that overlaps FGm while the FG2 and FG4 form the region that overlaps FGl. Furthermore, the medial-lateral transition wall between the FGl and FGm, which was predicted by our parcellation scheme, is close to the mid-fusiform sulcus, which corresponds to the cytoarchitectonic transition within the posterior FG and the mFG [Lorenz et al., 2015; Weiner et al., 2014]. The mid-fusiform sulcus is a stable anatomical landmark on the FG that can be clearly characterized after age seven [Weiner et al., 2014]. Because the subjects in this study were all healthy adults, identifying this stable landmark as the border that subdivides the FGl from the FGm via the probabilistic anatomical map is reasonable. In our study, the posterior boundary of the anterior subregion of the FG (FGa) is the anterior tip of the mid-fusiform sulcus, which is also the anterior boundary between the FGl and the FGm. This posterior boundary of FGa extended to the anterior tip of mFG which slightly overlapped with the anterior part of FG3 and bordered FG4 medially.

According to the whole brain functional connectivity map and the functional network connectivity fingerprints, the medial part of the posterior FG (FGm) is primarily positively correlated with the occipital pole and the posterior part of the medial temporal cortex. Consisting of the primary visual cortex and the extrastriate cortical areas, these regions are specialized for early visual processing [Crick and Koch, 1995], and two visual streams (dorsal and ventral) originate from here to the higher-order visual

areas [Goodale and Milner, 1992]. Thus, it could be postulated that the FGm may be involved in low-level visual processing and interacts with higher-order visual areas as a bridge to transmit visual stimuli information. Moreover, we found that the bilateral FGms were positively functionally connected to the auditory network, especially the superior temporal gyrus and posterior insula. It has been well established that the human perceptual system excels in combining multiple sensory signals, such as audio and visual signals, and that the posterior FG shows a higher functional activation in processing synchronous audio-visual signals than asynchronous audio-visual signals [Stevenson et al., 2010]. Another task-based fMRI study also confirmed that auditory emotion could remarkably affect facial perception [Jeong et al., 2011]. Those results suggested the FGm identified in our study may play a vital role in the integration of multiple stimuli.

The lateral part of the posterior FG (FGl) has been widely examined and has revealed its crucial role in dealing with various visual cognitions, such as face, word, and object recognition [Cohen et al., 2000; Kanwisher et al., 1997; Taylor et al., 2007; Wang et al., 2013]. In this study, different functional connectivity patterns were found between the bilateral FGls. Compared to the right FGl, the left FGl showed exclusively positive functional connectivity with brain regions corresponding to language processing. This was consistent with a previous investigation of functional lateralization in the FGl. Using task-based fMRI to detect neural priming also demonstrated that the left FGl was associated with the cerebral language network during word reading [Nakamura et al., 2007] and that a similar role of the left FGl has also been observed in the resting state [Zhao et al., 2011]. Taken together these findings suggested that the FGl is the core of an intrinsically organized functional network involved in word recognition and semantic processing. A recent study of the coactivation patterns of the FGl based on a meta-analytic connectivity analysis showed a lateralized pattern that was similar to the one identified in our results [Caspers et al., 2013a]. However, we found a less notable difference between the left and right FGls in functional connectivity with regions of visual-spatial processing. Unlike word recognition that occurs primarily in the left FGl, the visuospatial processing of the FGl, most often referred to as face recognition, is observed bilaterally [Gschwind et al., 2012; Kawasaki et al., 2012; Turk-Browne et al., 2010]. The hemispheric specialization of face perception in the FGl has been verified using various tasks, with the result that distinct facial information was found to be processed in different hemispheres and that a functional, hemispheric interaction occurs during this processing [Meng et al., 2012; Verosky and Turk-Browne, 2012]. In the resting state, the lateralization of facial processing in the FGl might be less obvious due to the lack of visual stimuli. Future studies should use various neuroimaging modalities to investigate the functional lateralization of this region.

From the whole brain functional connectivity maps, we found that the FGa was functionally correlated with the bilateral precuneus, posterior cingulate cortex, rostral part of the middle temporal gyrus, and middle occipital area. Previous fMRI studies revealed that the precuneus, posterior cingulate cortex, and middle temporal gyrus were more active in the resting state and with decreased activity than they were in the task state [Laird et al., 2009; Raichle et al., 2001]. The functional network connectivity fingerprints also indicated that the FGa was primarily connected with the default mode network (DMN). Interestingly, the DMN has been found to spatially and functionally overlap with the semantic memory system [Binder et al., 2009; Wirth et al., 2011], and the posterior part of the anterior FG showed high activation in connection with semantic cognition [Binder et al., 2011]. Additionally, a longitudinal pathway involved in semantic processing was observed in the temporal lobe, indicating that the posterior portions of the FG underpin stimulus-oriented semantic processing, whereas the anterior and middle portions were central to transmodal semantic processes [Visser et al., 2012]. Based on the connectivity patterns, we concluded that the FGa may be involved in high-level semantic processing of category information, such as faces or words, that is passed from the FGl. The behavioral domain and paradigm class profiles of the FGa in this study also revealed a higher probability of activation in semantic language cognition, another finding which supported our hypothesis.

To date, no consensus has been reached about functional organization in the FG. Various researchers have used task-based functional magnetic resonance imaging to report finding FG subregions such as the fusiform face area (FFA) [Grill-Spector et al., 2006; Hanson and Schmidt, 2011; Schwarzlose et al., 2005], fusiform body area (FBA) [Peelen and Downing, 2005; Weiner and Grill-Spector, 2010], and visual word form area (VWFA) [Cohen et al., 2000; Mei et al., 2010] and have debated the roles of each of these. In our study, these highly functional regions were all allocated to the FGl and seemed to share similar anatomical connection patterns. For example, our functional connectivity maps indicated the left FGl has the strong positive correlation with the left middle frontal gyrus where the VWFA consistently functionally coactivated [Liu et al., 2008], making it likely that the VWFA is located within the left FGl. Moreover, in the previous studies, the relationship of the FFA to the cytoarchitectonic FG subregions such as FG1/FG2 [Caspers et al., 2013b, 2014] and FG3/FG4 [Lorenz et al., 2015] were addressed in detail and they suggested that pFus-faces/FFA-1 located within FG2 and mFus-faces/FFA-2 fell within FG4 where all within the FGl in our parcellation scheme. Interestingly, even though initially the FFA was thought to be exclusively involved in human face detection and recognition instead of in detecting animal faces [Kanwisher et al., 1999] or nonface objects [Grill-Spector et al., 2004], Grill-Spector and her colleagues subsequently overturned their

own previous conclusion using high-resolution imaging. They found that the FG actually was functionally heterogeneous and that face-selective responses in this area showed no differences compared with nonface-selective responses [Grill-Spector et al., 2006]. It is well documented that the patterns of functional heterogeneity are to some extent constrained by the fiber connections in the brain [Eickhoff et al., 2010; Passingham et al., 2002]. Thus similarities in the anatomical connection patterns may explain the functional ambiguity of the FG subregions. However, the exact relationship between functional and structural connectivity needs to be further elucidated. Future studies should investigate this issue using the advantages of high-resolution MRI imaging.

## CONCLUSIONS

In summary, our results demonstrated that the human FG could be further subdivided into three functionally distinct parts based on distinct anatomical connectivity patterns. The medial portion (FGm) seems to be involved in low-level visual processing, and the lateral portion (FGl) may be related to high-level visual processing, such as categorical recognition. Finally, the anterior portion (FGa) appears to interact primarily with the semantic network. This functional organization supported two organizational transitions in the ventral temporal gyrus, the posterior/anterior direction of visual/semantic processing and the medial/lateral direction of low/high-level visual processing. To the best of our knowledge, this is the first study to evaluate the functional organization of the human FG based on its anatomical connections.

## ACKNOWLEDGMENTS

The authors thank Jinping Xu, Junjie Zhuo, Yu Zhang and Yaqin Zhang for useful suggestions about this research and also thank Rhoda E. and Edmund F. Perozzi for editing assistance. The authors declare that they have no competing financial interests.

## REFERENCES

Arcaro MJ, McMains SA, Singer BD, Kastner S (2009): Retinotopic organization of human ventral visual cortex. J Neurosci 29: 10638–10652.

Balsamo LM, Xu B, Gaillard WD (2006): Language lateralization and the role of the fusiform gyrus in semantic processing in young children. Neuroimage 31:1306–1314.

Beckmann M, Johansen-Berg H, Rushworth MF (2009): Connectivity-based parcellation of human cingulate cortex and its relation to functional specialization. J Neurosci 29:1175–1190.

Behrens TE, Woolrich MW, Jenkinson M, Johansen-Berg H, Nunes RG, Clare S, Matthews PM, Brady JM, Smith SM (2003): Characterization and propagation of uncertainty in diffusion-weighted MR imaging. Magn Reson Med 50:1077–1088.

Behrens TE, Berg HJ, Jbabdi S, Rushworth MF, Woolrich MW (2007): Probabilistic diffusion tractography with multiple fibre orientations: What can we gain? NeuroImage 34:144–155.

Binder JR, Desai RH, Graves WW, Conant LL (2009): Where is the semantic system? A critical review and meta-analysis of 120 functional neuroimaging studies. Cereb Cortex 19:2767–2796.

Binder JR, Gross WL, Allendorfer JB, Bonilha L, Chapin J, Edwards JC, Grabowski TJ, Langfitt JT, Loring DW, Lowe MJ, Koenig K, Morgan PS, Ojemann JG, Rorden C, Szaflarski JP, Tivarus ME, Weaver KE (2011): Mapping anterior temporal lobe language areas with fMRI: A multicenter normative study. Neuroimage 54:1465–1475.

Biswal BB, Mennes M, Zuo XN, Gohel S, Kelly C, Smith SM, Beckmann CF, Adelstein JS, Buckner RL, Colcombe S, Dogonowski AM, Ernst M, Fair D, Hampson M, Hoptman MJ, Hyde JS, Kiviniemi VJ, Kotter R, Li SJ, Lin CP, Lowe MJ, Mackay C, Madden DJ, Madsen KH, Margulies DS, Mayberg HS, McMahon K, Monk CS, Mostofsky SH, Nagel BJ, Pekar JJ, Peltier SJ, Petersen SE, Riedl V, Rombouts SA, Rypma B, Schlaggar BL, Schmidt S, Seidler RD, Siegle GJ, Sorg C, Teng GJ, Veijola J, Villringer A, Walter M, Wang L, Weng XC, Whitfield-Gabrieli S, Williamson P, Windischberger C, Zang YF, Zhang HY, Castellanos FX, Milham MP (2010): Toward discovery science of human brain function. Proc Natl Acad Sci USA 107:4734–4739.

Brewer AA, Liu J, Wade AR, Wandell BA (2005): Visual field maps and stimulus selectivity in human ventral occipital cortex. Nat Neurosci 8:1102–1109.

Caspers J, Zilles K, Amunts K, Laird AR, Fox PT, Eickhoff SB (2013a): Functional characterization and differential coactivation patterns of two cytoarchitectonic visual areas on the human posterior fusiform gyrus. Hum Brain Mapp 35: 2754–2767.

Caspers J, Zilles K, Eickhoff SB, Schleicher A, Mohlberg H, Amunts K (2013b): Cytoarchitectonical analysis and probabilistic mapping of two extrastriate areas of the human posterior fusiform gyrus. Brain Struct Funct 218:511–526.

Caspers J, Zilles K, Amunts K, Laird AR, Fox PT, Eickhoff SB (2014): Functional characterization and differential coactivation patterns of two cytoarchitectonic visual areas on the human posterior fusiform gyrus. Hum Brain Mapp 35:2754–2767.

Cohen L, Dehaene S, Naccache L, Lehericy S, Dehaene-Lambertz G, Henaff MA, Michel F (2000): The visual word form area: Spatial and temporal characterization of an initial stage of reading in normal subjects and posterior split-brain patients. Brain 123:291–307.

Crick F, Koch C (1995): Are we aware of neural activity in primary visual cortex? Nature 375:121–123.

Dehaene S, Naccache L, Cohen L, Bihan DL, Mangin JF, Poline JB, Riviere D (2001): Cerebral mechanisms of word masking and unconscious repetition priming. Nat Neurosci 4:752–758.

Deng F, Jiang X, Zhu D, Zhang T, Li K, Guo L, Liu T (2014): A functional model of cortical gyri and sulci. Brain Struct Funct 219:1473–1491.

Desikan RS, Segonne F, Fischl B, Quinn BT, Dickerson BC, Blacker D, Buckner RL, Dale AM, Maguire RP, Hyman BT, Albert MS, Killiany RJ (2006): An automated labeling system for subdividing the human cerebral cortex on MRI scans into gyral based regions of interest. Neuroimage 31:968–980.

Destrieux C, Fischl B, Dale A, Halgren E (2010): Automatic parcellation of human cortical gyri and sulci using standard anatomical nomenclature. NeuroImage 53:1–15.

Eickhoff SB, Jbabdi S, Caspers S, Laird AR, Fox PT, Zilles K, Behrens TE (2010): Anatomical and functional connectivity of cytoarchitectonic areas within the human parietal operculum. J Neurosci 30:6409–6421.

Fan L, Wang J, Zhang Y, Han W, Yu C, Jiang T (2013): Connectivity-Based Parcellation of the Human Temporal Pole Using Diffusion Tensor Imaging. Cereb Cortex.

Goodale MA, Milner AD (1992): Separate visual pathways for perception and action. Trends Neurosci 15:20–25.

Grill-Spector K, Knouf N, Kanwisher N (2004): The fusiform face area subserves face perception, not generic within-category identification. Nat Neurosci 7:555–562.

Grill-Spector K, Sayres R, Ress D (2006): High-resolution imaging reveals highly selective nonface clusters in the fusiform face area. Nat Neurosci 9:1177–1185.

Gschwind M, Pourtois G, Schwartz S, Van De Ville D, Vuilleumier P (2012): White-matter connectivity between face-responsive regions in the human brain. Cereb Cortex 22:1564–1576.

Hanson SJ, Schmidt A (2011): High-resolution imaging of the fusiform face area (FFA) using multivariate non-linear classifiers shows diagnosticity for non-face categories. NeuroImage 54: 1715–1734.

Jeong JW, Diwadkar VA, Chugani CD, Sinsoongsud P, Muzik O, Behen ME, Chugani HT, Chugani DC (2011): Congruence of happy and sad emotion in music and faces modifies cortical audiovisual activation. Neuroimage 54:2973–2982.

Kanwisher N, McDermott J, Chun MM (1997): The fusiform face area: A module in human extrastriate cortex specialized for face perception. J Neurosci 17:4302–4311.

Kanwisher N, Stanley D, Harris A (1999): The fusiform face area is selective for faces not animals. Neuroreport 10:183–187.

Kanwisher N, Yovel G (2006): The fusiform face area: a cortical region specialized for the perception of faces. Philos Trans R Soc Lond B Biol Sci 361:2109–2128.

Kawasaki H, Tsuchiya N, Kovach CK, Nourski KV, Oya H, Howard MA, Adolphs R (2012): Processing of facial emotion in the human fusiform gyrus. J Cogn Neurosci 24:1358–1370.

Kolster H, Peeters R, Orban GA (2010): The retinotopic organization of the human middle temporal area MT/V5 and its cortical neighbors. J Neurosci 30:9801–9820.

Laird AR, Eickhoff SB, Li K, Robin DA, Glahn DC, Fox PT (2009): Investigating the functional heterogeneity of the default mode network using coordinate-based meta-analytic modeling. J Neurosci 29:14496–14505.

Liu C, Zhang WT, Tang YY, Mai XQ, Chen HC, Tardif T, Luo YJ (2008): The Visual Word Form Area: Evidence from an fMRI study of implicit processing of Chinese characters. NeuroImage 40:1350–1361.

Lorenz S, Weiner KS, Caspers J, Mohlberg H, Schleicher A, Bludau S, Eickhoff SB, Grill-Spector K, Zilles K, Amunts K (2015): Two new cytoarchitectonic areas on the human midfusiform gyrus. Cereb Cortex bhv225.

Mars RB, Sallet J, Schuffelgen U, Jbabdi S, Toni I, Rushworth MF (2012): Connectivity-based subdivisions of the human right "temporoparietal junction area": Evidence for different areas participating in different cortical networks. Cereb Cortex 22: 1894–1903.

Mei L, Xue G, Chen C, Xue F, Zhang M, Dong Q (2010): The "visual word form area" is involved in successful memory encoding of both words and faces. NeuroImage 52:371–378.

Meng M, Cherian T, Singal G, Sinha P (2012): Lateralization of face processing in the human brain. Proc Biol Sci 279: 2052–2061.

Mion M, Patterson K, Acosta-Cabronero J, Pengas G, Izquierdo-Garcia D, Hong YT, Fryer TD, Williams GB, Hodges JR, Nestor PJ (2010): What the left and right anterior fusiform gyri tell us about semantic memory. Brain 133:3256–3268.

Nakamura K, Dehaene S, Jobert A, Le Bihan D, Kouider S (2007): Task-specific change of unconscious neural priming in the cerebral language network. Proc Natl Acad Sci USA 104:19643–19648.

Nie J, Guo L, Li K, Wang Y, Chen G, Li L, Chen H, Deng F, Jiang X, Zhang T, Huang L, Faraco C, Zhang D, Guo C, Yap PT, Hu X, Li G, Lv J, Yuan Y, Zhu D, Han J, Sabatinelli D, Zhao Q, Miller LS, Xu B, Shen P, Platt S, Shen D, Hu X, Liu T (2012): Axonal fiber terminations concentrate on gyri. Cereb Cortex 22:2831–2839.

Passingham RE, Stephan KE, Kotter R (2002): The anatomical basis of functional localization in the cortex. Nat Rev Neurosci 3:606–616.

Peelen MV, Downing PE (2005): Selectivity for the human body in the fusiform gyrus. J Neurophysiol 93:603–608.

Price CJ, Devlin JT (2003): The myth of the visual word form area. NeuroImage 19:473–481.

Raichle ME, MacLeod AM, Snyder AZ, Powers WJ, Gusnard DA, Shulman GL (2001): A default mode of brain function. Proc Natl Acad Sci USA 98:676–682.

Schwarzlose RF, Baker CI, Kanwisher N (2005): Separate face and body selectivity on the fusiform gyrus. J Neurosci 25: 11055–11059.

Schwarzlose RF, Swisher JD, Dang S, Kanwisher N (2008): The distribution of category and location information across object-selective regions in human visual cortex. Proc Natl Acad Sci USA 105:4447–4452.

Sergent J, Ohta S, MacDonald B (1992): Functional neuroanatomy of face and object processing. A positron emission tomography study. Brain 115:15–36.

Smith SM, Fox PT, Miller KL, Glahn DC, Fox PM, Mackay CE, Filippini N, Watkins KE, Toro R, Laird AR, Beckmann CF (2009): Correspondence of the brain's functional architecture during activation and rest. Proc Natl Acad Sci USA 106:13040–13045.

Stevenson RA, Altieri NA, Kim S, Pisoni DB, James TW (2010): Neural processing of asynchronous audiovisual speech perception. Neuroimage 49:3308–3318.

Taylor JC, Wiggett AJ, Downing PE (2007): Functional MRI analysis of body and body part representations in the extrastriate and fusiform body areas. J Neurophysiol 98:1626–1633.

Turk-Browne NB, Norman-Haignere SV, McCarthy G (2010): Face-specific resting functional connectivity between the fusiform gyrus and posterior superior temporal sulcus. Front Hum Neurosci 4:176.

Verosky SC, Turk-Browne NB (2012): Representations of facial identity in the left hemisphere require right hemisphere processing. J Cogn Neurosci 24:1006–1017.

Visser M, Jefferies E, Embleton KV, Lambon Ralph MA (2012): Both the middle temporal gyrus and the ventral anterior temporal area are crucial for multimodal semantic processing: Distortion-corrected fMRI evidence for a double gradient of information convergence in the temporal lobes. J Cogn Neurosci 24:1766–1778.

Wang J, Fan L, Zhang Y, Liu Y, Jiang D, Yu C, Jiang T (2012): Tractography-based parcellation of the human left inferior parietal lobule. Neuroimage 63:641–652.

Wang X, Han Z, He Y, Caramazza A, Song L, Bi Y (2013): Where color rests: Spontaneous brain activity of bilateral fusiform and lingual regions predicts object color knowledge performance. NeuroImage 76:252–263.

Weiner KS, Grill-Spector K (2010): Sparsely-distributed organization of face and limb activations in human ventral temporal cortex. NeuroImage 52:1559–1573.

Weiner KS, Golarai G, Caspers J, Chuapoco MR, Mohlberg H, Zilles K, Amunts K, Grill-Spector K (2014): The mid-fusiform sulcus: A landmark identifying both cytoarchitectonic and functional divisions of human ventral temporal cortex. Neuroimage 84:453–465.

Wirth M, Jann K, Dierks T, Federspiel A, Wiest R, Horn H (2011): Semantic memory involvement in the default mode network: A functional neuroimaging study using independent component analysis. Neuroimage 54:3057–3066.

Zhang Y, Fan L, Wang J, Zhu M, Yu C, Jiang T (2014): Connectivity-based parcellation of the human posteromedial cortex. Cereb Cortex 24:719–727.

Zhao J, Liu J, Li J, Liang J, Feng L, Ai L, Lee K, Tian J (2011): Intrinsically organized network for word processing during the resting state. Neurosci Lett 487:27–31.